

Independence of the Inverse Spin Hall Effect with the Magnetic Phase in Thin NiCu Films

Sara Varotto,^{1,2,‡} Maxen Cosset-Chéneau,¹ Cécile Grèzes,¹ Yu Fu,¹ Patrick Warin,¹ Ariel Brenac,¹ Jean-François Jacquot,³ Serge Gambarelli,³ Christian Rinaldi,² Vincent Baltz,¹ Jean-Philippe Attané,^{1,*} Laurent Vila,¹ and Paul Noël^{1,†}
¹Université Grenoble Alpes, CEA, CNRS, Grenoble INP, SPINTEC, F-38000 Grenoble, France
²Department of Physics, Politecnico di Milano, 20133 Milano, Italy
³Université Grenoble Alpes, CEA, SYMMES, F-38000 Grenoble, France



(Received 15 May 2020; revised 8 September 2020; accepted 20 November 2020; published 31 December 2020)

Large spin Hall angles have been observed in $3d$ ferromagnets, but their origin, and especially their link with the ferromagnetic order, remain unclear. Here, we investigate the evolution of the inverse spin Hall effect of $\text{Ni}_{60}\text{Cu}_{40}$ and $\text{Ni}_{50}\text{Cu}_{50}$ across their Curie temperatures using spin-pumping experiments. We show that the inverse spin Hall effect in these samples is comparable to that of platinum, and that it is insensitive to the magnetic order. These results point toward a Heisenberg localized model of the transition and suggest that the large spin Hall effects in $3d$ ferromagnets can be independent of the magnetic phase.

DOI: [10.1103/PhysRevLett.125.267204](https://doi.org/10.1103/PhysRevLett.125.267204)

Heavy metals and dilute alloys with heavy metal impurities offer large spin Hall angles (SHA), as the spin Hall effect (SHE) is closely related to the spin-orbit coupling [1]. This has motivated a considerable experimental and theoretical effort toward the study of SHE in $5d$ materials and their alloys [2–8]. Despite the weaker spin-orbit coupling [9], large SHAs, comparable to that of Pt, can also be obtained in $3d$ ferromagnetic metals [10–14]. The ferromagnetic material can even have a strong contribution to the SHE measured in ferromagnet and heavy metal bilayers, through the self-induced SHE [15,16] or the anomalous spin-orbit torque [17]. The spin-orbit coupling is at the origin of specific transport properties in ferromagnets. Its interplay with magnetism gives rise to the anisotropic magnetoresistance [18] and the anomalous Hall effect [19]. However, in ferromagnetic metals, the link between the SHE and the magnetic order is unclear.

Recent theoretical [20,21] and experimental works [22] showed the existence of two contributions to the SHE in a ferromagnet: a magnetization-independent effect, usually called spin Hall effect, and a magnetization-direction dependent one, known as the anomalous spin Hall effect. When the spin polarization of the spin current is aligned with the magnetization, both terms are expected to contribute, and the overall effect is named longitudinal spin Hall effect (LSHE) [23]. In a ferromagnetic material the modifications of the band structure at the phase transition [24–26], such as the band shift associated with the vanishing of the exchange splitting [27], could lead to a change in the spin Hall properties. The investigation of the SHE, or of its reciprocal effects: the inverse spin Hall effect (ISHE) in the paramagnetic state, and the inverse longitudinal spin Hall effect (ILSHE) in the ferromagnetic state would therefore provide further insight

about the relation between the magnetic order and the spin Hall effect.

The influence of the ferromagnetic phase transition on SHE has been studied in dilute magnetic alloys in a $4d$ or $5d$ matrix. The enhancement of the SHA at the Curie temperature in $\text{Ni}_{0.09}\text{Pd}_{0.91}$ [28] or $\text{Fe}_{0.25}\text{Pt}_{0.75}$ [29] was attributed to the skew scattering on magnetic impurities associated with spin fluctuations [30]. In these alloys, except in the vicinity of the transition temperature, the conversion mechanism is dominated by that of Pt or Pd, and the magnetic order plays a little role in the SHE. In another ferromagnetic system, a $4d$ oxide, SrRuO_3 (SRO) the effect of the phase transition on the SHE has been reported to be either strong [31] or very weak [32].

In this study, we investigate $3d$ alloys of NiCu with a stoichiometry dependent Curie temperature [33,34]. The importance of the spin-orbit interaction in this system is known since the first experimental development of the Valet-Fert model [35]. More recently, Keller *et al.* [25] showed that a large SHA could be obtained in NiCu, making it an ideal system to study the effect of the ferromagnetic-paramagnetic transition.

Here, we measure the temperature dependence of the inverse spin Hall effect of NiCu alloys using spin pumping by ferromagnetic resonance. First, we show that it is essential to avoid a direct magnetic coupling between the ferromagnetic spin injector and the NiCu below its Curie temperature, as it generates profound modifications of the magnetization dynamics and hinders accurate measurements. For this purpose, we used a thin Cu layer to suppress the coupling. For two different stoichiometries, we demonstrate that the SHE in NiCu is large and independent of the magnetic state. This result indicates that the spin Hall effect in light metal alloys of $3d$ magnetic

elements hold potential for large conversion efficiencies, in both their paramagnetic and ferromagnetic phases.

To perform the spin-pumping measurements, we used $\text{Co}_{53}\text{Fe}_{27}\text{B}_{20}$ (CFB) as a spin injector, because its Gilbert damping, magnetization, and resistivity [36] are nearly temperature independent in the studied temperature range, and since its self-induced SHE is small [16]. Using magnetron sputtering, we grew a 15 nm thick CFB layer onto a SiSiO_2 substrate. The NiCu layer was sputtered on top, directly from $\text{Ni}_{60}\text{Cu}_{40}$ and $\text{Ni}_{50}\text{Cu}_{50}$ targets. The samples were further protected from oxidation by a 3 nm Al layer. To compare the spin to charge conversion efficiency of NiCu with that of platinum, we also grew a CFB(15)/Pt(15)/Al(3) sample (the numbers in parenthesis indicates the thicknesses in nm), using the same deposition chamber. The samples were cut into slabs of length $L = 2.4$ mm and width $W = 0.4$ mm.

The spin-pumping measurements were performed in a Bruker ESP300E X-band CW with a 4118X-MS5 resonator at a fixed frequency of 9.7 GHz, using the same measurement geometry as in Ref. [37]. Following the theory of spin pumping, at the ferromagnetic resonance a spin current is injected from the ferromagnetic layer toward the attached layer [38]. This spin current is then converted into a charge current through ISHE, detected as a voltage in open circuit conditions [2]. As the measured voltage is proportional to both the square of the radiofrequency magnetic field h_{rf} and the total longitudinal resistance of the sample R [37], we compare these samples on the basis of the normalized spin-pumping signal V/Rh_{rf}^2 . The amplitude of h_{rf}^2 was determined before every measurement by measuring the Q factor of the resonant cavity with the sample placed inside [39].

Remarkably, the spin-pumping signal in CFB/NiCu has the same sign and a similar amplitude as in the CFB/Pt sample as can be seen in Fig. 1(a). The signal is dominated by a symmetric contribution V_{sym} , suggesting that it originates from the ISHE as further confirmed by the out-of-plane angular dependence [40–44]

We also performed broadband FMR measurements from 4 to 24 GHz using a broadband stripline with lock-in detection. By applying the Kittel formula $f_{\text{res}} = (\mu_0\gamma/2\pi)\sqrt{(M_s + H_{\text{res}} + H_k)(H_{\text{res}} + H_k)}$, with f_{res} the resonance frequency, H_{res} the resonance field, μ_0 the vacuum permeability, γ the gyromagnetic ratio, H_k the anisotropy field, and M_s the effective magnetization of the thin film, we extracted the magnetic properties of the CFB film. The obtained values are similar in all films and close to previous observations in $\text{Co}_{53}\text{Fe}_{27}\text{B}_{20}$, with an effective magnetization of 890 ± 20 kA/m, and a gyromagnetic ratio of $(1.870 \pm 0.005) \times 10^{11}$ rad s⁻¹ T⁻¹ ($g = 2.130 \pm 0.005$). We extracted the Gilbert damping α from the frequency dependence of the peak-to-peak linewidth ΔH_{pp} using $\mu_0\Delta H_{\text{pp}} = (2/\sqrt{3})(2\pi\alpha f/\gamma) + \mu_0\Delta H_0$, where ΔH_0 is the inhomogeneous broadening.

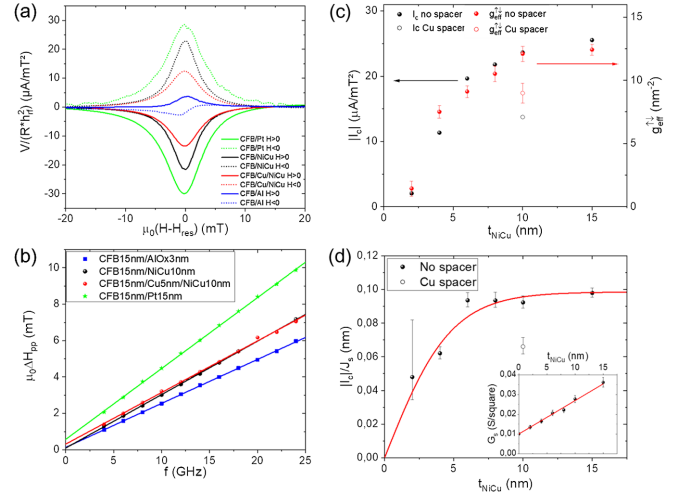


FIG. 1. (a) Spin-pumping signals in CFB(15)/Pt(15), CFB(15)/ $\text{Ni}_{60}\text{Cu}_{40}$ (10), CFB(15)/Cu(5)/ $\text{Ni}_{60}\text{Cu}_{40}$ (10), and in the CFB(15)/Al(3) reference sample. The signals are given in the parallel ($H > 0$) and antiparallel ($H < 0$) configurations. (b) Broadband measurement of the FMR linewidth of CFB(15)/Al(3), CFB(15)/ $\text{Ni}_{60}\text{Cu}_{40}$ (10), CFB(15)/Cu(5)/ $\text{Ni}_{60}\text{Cu}_{40}$ (10), and CFB(15)/Pt(15) samples. (c) Effective spin mixing conductance and absolute value of the charge current production, as a function of the NiCu film thickness t_{NiCu} . (d) Thickness dependence of the absolute value of the charge current production divided by the spin current. The fit in red is performed using Eq. (2). The inset shows the thickness dependence of the sheet conductance. The measurements were performed at room temperature, all thicknesses are in nm.

As can be seen in Fig. 1(b) an enhancement of the damping is observed from $(6.64 \pm 0.03) \times 10^{-3}$ in CFB(15)/Al(3) to $(8.05 \pm 0.05) \times 10^{-3}$ in CFB(15)/ $\text{Ni}_{60}\text{Cu}_{40}$ (10) or $(1.070 \pm 0.006) \times 10^{-2}$ in CFB(15)/Pt(15). The damping enhancement known as extra-damping $\Delta\alpha$ suggests the existence of spin injection via spin pumping [45], and possibly to other effects such as magnetic proximity [46] and spin memory loss (SML) [39].

We performed cavity spin pumping as well as broadband measurements as a function of the thickness of the $\text{Ni}_{60}\text{Cu}_{40}$ layer (from 2 to 15 nm), to evaluate both the spin diffusion length λ_s and the spin Hall angle θ_{SHE} . The broadband FMR measurement at room temperature shows that the extracted magnetic properties of the CFB are unaffected by the NiCu layer, except for the damping that increases with the NiCu thickness saturating at 10 nm [40]. The absence of a sharp increase of the damping in ultrathin NiCu layers is not compatible with a large SML or proximity effect. We also grew a sample with a 5 nm insertion of Cu between the CFB and NiCu in order to suppress any magnetic proximity effects [46]. The spin signal is lowered with the spacer as can be seen in Fig. 1(a) possibly due to SML at the CoFeB/Cu interface. The damping is slightly reduced from $(8.05 \pm 0.05) \times 10^{-3}$ to $(7.75 \pm 0.1) \times 10^{-3}$, as shown in Fig. 1(b), showing

evidence of the minor role of the magnetic proximity effect in the damping enhancement. From the broadband FMR measurement we calculate the effective spin mixing conductance $g_{\text{eff}}^{\uparrow\downarrow} = (4\pi M_s t_{\text{FM}}/\gamma\hbar)\Delta\alpha$, with t_{FM} the thickness of the ferromagnetic layer, and \hbar the reduced Planck constant. The obtained values of $g_{\text{eff}}^{\uparrow\downarrow}$, as well as the absolute value of the charge current production at resonance $I_c = \{[V_{\text{sym}}(H > 0) - V_{\text{sym}}(H < 0)]/2Rh_{\text{rf}}^2\}$, are plotted in Fig. 1(c) with and without the Cu spacer. The small contribution of CFB to the spin-pumping signal was separately determined on CFB(15)/Al(3) layer [Fig. 1(a)] and subtracted. The spin mixing conductance and spin-pumping signal saturate at 10 nm with a value of $12.4 \pm 0.4 \text{ nm}^{-2}$ and $25 \mu\text{A}/\text{mT}^2$, respectively. Owing to the apparent minor role of magnetic proximity effect and SML in the CFB/NiCu bilayers, we evaluate the spin current using the conventional spin-pumping model [37,38]:

$$J_s = \frac{g_{\text{eff}}^{\uparrow\downarrow}\gamma^2\hbar h_{\text{rf}}^2}{8\pi\alpha^2} \left(\frac{\mu_0 M_s \gamma + \sqrt{(\mu_0 M_s \gamma)^2 + 4\omega^2}}{(\mu_0 M_s \gamma)^2 + 4\omega^2} \right) \left(\frac{2e}{\hbar} \right). \quad (1)$$

The resistivity ρ of the NiCu layer is of $60 \pm 3 \mu\Omega \text{ cm}$, and independent on the thickness [cf. inset of Fig. 1(d)], in line with the short mean free path in this alloy [47]. We can thus assume a constant spin diffusion length and spin Hall angle. The charge current as a function of the NiCu thickness is then given by

$$I_c(t) = W\theta_{\text{SHE}}\lambda_s J_s \tanh\left(\frac{t_{\text{NiCu}}}{2\lambda_s}\right). \quad (2)$$

Combining Eqs. (1) and (2) it is possible to extract λ_s and θ_{SHE} . From the fit in Fig. 1(d) we obtained $\lambda_s = 2.4 \pm 0.3 \text{ nm}$ and $\theta_{\text{SHE}} = 4.1_{-0.4}^{+0.6}\%$. Contrary to Ref. [25], we did not observe any remarkable SML or magnetic proximity effect, which might explain why our estimated SHA is much lower. The value of I_c/J_s is 32% smaller with the Cu interlayer compared to the case of the direct contact. This is likely due to the SML which is typically of 20% to 30% in CoFe/Cu [48] and Co/Cu [49].

In order to investigate the effect of the NiCu phase transition, we performed a temperature dependence of the spin pumping with and without Cu insertion in samples with 10 nm thick NiCu.

Figure 2(a) clearly shows that the resonant properties of both samples are similar around room temperature, but their behaviors at low temperature are strikingly different. In the absence of the Cu interlayer, the resonance field decreases below 210 K, while the linewidth increases. These effects are not observed with the 5 nm Cu spacer. This change occurs around the expected paramagnetic to ferromagnetic transition temperature of $\text{Ni}_{60}\text{Cu}_{40}$ [33,34] of about $T_c = 210 \pm 5 \text{ K}$, as confirmed by AHE and resistivity measurements [40]. The value of T_c is not

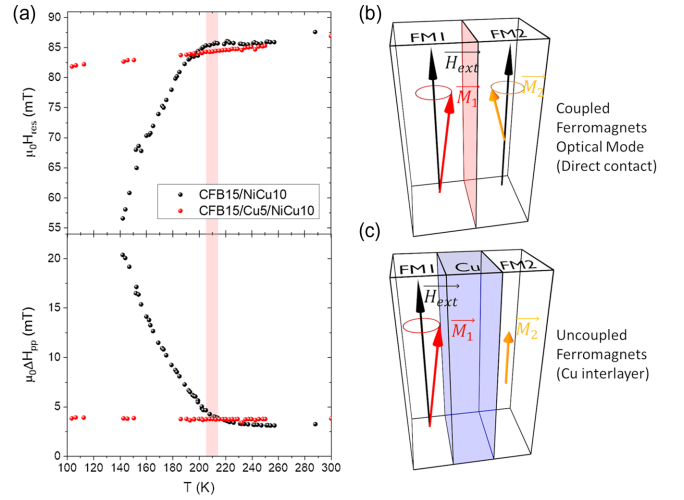


FIG. 2. (a) Resonance field and linewidth of CFB as a function of the temperature in CFB(15)/ $\text{Ni}_{60}\text{Cu}_{40}$ (10) and CFB(15)/Cu(5)/ $\text{Ni}_{60}\text{Cu}_{40}$ (10). The red shaded area depicts the Curie temperature T_c ($210 \pm 5 \text{ K}$) of $\text{Ni}_{60}\text{Cu}_{40}$. (b) In direct contact at resonance both magnetization vectors of FM1 (CFB) and FM2 (NiCu) precess out of phase for the optical mode. (c) When the ferromagnets are decoupled using a thick enough Cu interlayer only FM1, here CFB, is excited at its resonance.

affected by the deposition of Cu or by the proximity with a ferromagnet, contrary to previous work [50].

When CoFeB is in direct contact with NiCu and below T_c , an exchange coupling between the two layers arises, so that the magnetization vectors of the two ferromagnets precess together either in phase (acoustic mode) or out of phase (optical mode). The spin transport can be of a magnonic nature and is not limited to electrons [51], leading to strong modifications of the resonance field and linewidth [51–53]. The lowering of the resonance field in Fig. 2(a) is associated to the optical mode (out of phase precession) depicted in Fig. 2(b). Such a decrease becomes larger when the temperature is lowered, due to both the increased magnetization of NiCu and the strengthening of the exchange coupling. With the 5 nm Cu spacer the coupling is suppressed and the electronic transport prevails. The suppression of the coupling is revealed by the absence of any noticeable change of the resonance field and linewidth around the Curie temperature seen in Fig. 2, and confirmed by additional AHE measurements [40]. As the two magnetic layers are not coupled, when CFB is at resonance the magnetization of NiCu is out of resonance (i.e., static) as depicted in Fig. 2(c), so that the dynamical properties remain unaffected [54]. We could not observe the resonance of $\text{Ni}_{60}\text{Cu}_{40}$ in the uncoupled case or the acoustic mode in direct contact either using the lock-in detection of the spectrometer and the electrical detection. This is likely due to the broad linewidth of the resonance peak of NiCu [55] (see Supplemental Material [40]).

The charge current production at resonance I_c as a function of the temperature was measured, with and

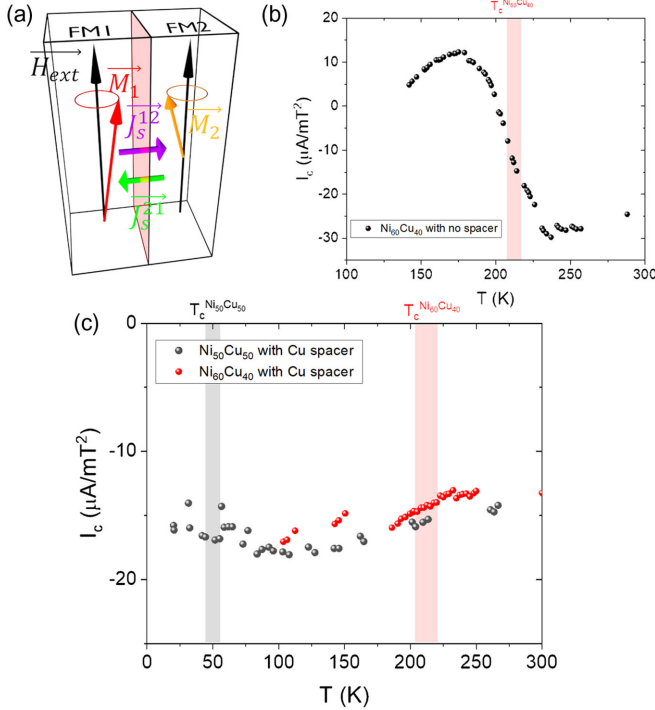


FIG. 3. (a) Schematic representation of the spin-pumping process below T_c (optical mode) for the direct contact. Spin currents are injected from FM1 to FM2 (J_s^{12}) and from FM2 to FM1 (J_s^{21}) with a 180° phase shift. (b) Spin-pumping signal in a coupled bilayer without Cu spacer. In red the T_c of $Ni_{60}Cu_{40}$. (c) ISHE signal as a function of temperature in CFB(15)/Cu(5)/ $Ni_{60}Cu_{40}$ (10) and CFB(15)/Cu(5)/ $Ni_{50}Cu_{50}$ (10) samples with different Curie temperatures ($T_c^{Ni_{60}Cu_{40}}$ shown in red and $T_c^{Ni_{50}Cu_{50}}$ in gray).

without Cu insertion. As can be seen in Fig. 3(a), in the exchange-coupled system without the Cu insertion I_c is negative above the Curie temperature, but when lowering the temperature, the current production is abruptly modified around T_c , and even changes sign below 200 K. Without further measurements, one might conclude that the SHE is strongly affected by the ferromagnetic transition, and changes sign on a narrow temperature range. However, in the case of the direct contact, the strong modification of the resonance properties across the magnetic phase transition makes it impossible to accurately evaluate the spin current injected at resonance. Moreover, the CoFeB and NiCu layers are coupled and both precessing at resonance, so that a spin current is injected from CFB toward NiCu and from NiCu toward CFB, as depicted in Fig. 3(b). The exact spin accumulation profile cannot be evaluated, and a non-negligible ISHE signal from CFB could start contributing [13].

For these reasons, to properly evaluate the ISHE in NiCu below the Curie temperature, it is necessary to perform the same measurement in the CFB/Cu/NiCu trilayer to verify that such sign a change is not due to spurious effects related to the coupling. In this configuration, below T_c the

magnetization of NiCu and the injected spins are parallel, the measured signal is the inverse longitudinal spin Hall effect. In the decoupled system, I_c is constant and does not change sign at T_c , as can be seen in Fig. 3(c). Similarly to what is observed at RT the reduced value of the produced charge current with the Cu spacer is likely due to the SML. The absence of any noticeable effect of the transition is also observed for another stoichiometry $Ni_{50}Cu_{50}$ ($T_c = 60$ K). In these trilayers the spin signal as well as the resonant properties of the CFB layer are independent of the temperature: the same spin current injection and charge production are observed in both the paramagnetic and the ferromagnetic states. We could not observe any anomaly around the Curie temperature evidencing the SHE mechanism differs from that of NiPd [28]. Therefore, the large ISHE in NiCu alloys in the paramagnetic phase is equal to the ILSHE in the ferromagnetic phase, and thus unrelated to the magnetic order.

We observed that the spin Hall angle is positive while the anomalous Hall angle is negative [40], in agreement with the calculations of the intrinsic effects in ferromagnetic Ni [17,20,21]. This suggests that the two mechanisms in NiCu are dominated by the intrinsic contribution. It also confirms previous observations by Omori *et al.* that the anomalous and spin Hall effect can be of opposite sign [14]. For both $Ni_{60}Cu_{40}$ and $Ni_{50}Cu_{50}$, the figure of merit of the spin to charge current conversion $\theta_{SHE}\lambda_s$ is of 0.1 nm, independently on the stoichiometry, as expected for alloys of similar resistivity [8]. This value is comparable to that of Pt (0.18 nm) [39,56], thereby allowing for efficient detection of spin currents. In order to evaluate the possible contribution of a magnetization-direction dependent SHE, we also performed an out of plane angular dependence in CFB/Cu/ $Ni_{60}Cu_{40}$ at 100 K. It appears that the non-collinearity of the magnetization and the injected spins plays a limited role in the ISHE of magnetic NiCu [40].

The large SHA in paramagnetic NiCu was previously explained by similarities between the calculated band structure of paramagnetic nickel and platinum around the Fermi level [25]. Nonetheless, the calculated band structure of ferromagnetic nickel in Ref. [25] does not resemble that of Pt. This is not compatible with our observation of a large magnetic phase independent ISHE in NiCu. On the contrary, our observations suggest that the band structure is not particularly affected by the phase transition, or that these possible changes do not reflect in a modification of the spin Hall effect properties. The modifications of the band structure occurring at the ferromagnetic transition and in particular the shift of the bands associated with the collapse of the exchange splitting are still debated with conflicting results for nickel [27,57,58]. The ferromagnetic-paramagnetic transition is characterized by the loss of the long-range ferromagnetic order but is not necessarily associated with the collapse of exchange splitting that occurs at higher temperature as observed in

SrRuO₃ or Fe [59,60]. The observation of a phase independent SHE indicates that the itinerant Stoner model of ferromagnetism does not describe well the ferromagnetic-paramagnetic phase transition in NiCu. The observed behavior points toward a localized character of the magnetism (Heisenberg-like) in NiCu alloys, in line with previous experimental and theoretical results showing that local moments associated to the nearest neighbor environment of nickel atoms are at the origin of magnetism [61,62]. Thus, our experimental results could be explained by the similarity of the band structure of NiCu in the paramagnetic and ferromagnetic phase.

In summary, using spin-pumping FMR in CFB/Cu/NiCu with two different stoichiometries, we measured a large positive spin Hall angle in NiCu comparable to the one of Pt. The SHA is insensitive to the magnetic phase when magnetization and injected spins are aligned. This suggests that, in NiCu, the effect of the ferromagnetic-paramagnetic transition on the SHE has to be understood using a localized picture. We emphasized the importance of avoiding direct contact to properly measure the ISHE in a ferromagnet for resonance measurements. Direct contact leads to drastic changes in the dynamic response that are hard to estimate. This might explain the discrepancy between measurements of the spin Hall effect in the same material but in contact with different ferromagnets [29,31]. Moreover, our results show that the ferromagnetic order does not necessarily play a key role in the large spin Hall effect of ferromagnets. A large variety of alloys composed of Ni, Co, or Fe in the ferromagnetic or paramagnetic phase could therefore be explored as spin current generators and detectors, extending the number of possible light metal systems with a large SHE.

We acknowledge the financial support by ANR French National Research Agency Toprise (ANR-16-CE24-0017), ANR French National Research Agency OISO (ANR-17-CE24-0026), Laboratoire d'excellence LANEF (ANR-10-LABX-51-01), and the Fondazione Cariplo and Regione Lombardia, Grant No. 2017-1622 (ECOS). We are grateful to the EPR facilities available at the national TGE RPE facilities (IR 3443). We thank Christian Lombard and Vincent Maurel for their help and advice on the FMR measurement setup. Interesting discussions with Yasuhiro Niimi are gratefully acknowledged.

S. Varotto and M. Cosset-Chéneau contributed equally to this work.

*Corresponding author.
jean-philippe.attane@cea.fr

†Corresponding author.
paul.noel@mat.ethz.ch
Present address: Department of Materials, ETH Zurich,
8093 Zurich, Switzerland.

‡Present address: Unité Mixte de Physique, CNRS, Thales, Université Paris-Saclay, 91767 Palaiseau, France.

- [1] J. Sinova, S. O. Valenzuela, J. Wunderlich, C. H. Back, and T. Jungwirth, *Rev. Mod. Phys.* **87**, 1213 (2015).
- [2] E. Saitoh, M. Ueda, H. Miyajima, and G. Tatara, *Appl. Phys. Lett.* **88**, 182509 (2006).
- [3] T. Kimura, Y. Otani, T. Sato, S. Takahashi, and S. Maekawa, *Phys. Rev. Lett.* **98**, 156601 (2007).
- [4] T. Tanaka, H. Kontani, M. Naito, T. Naito, D. S. Hirashima, K. Yamada, and J. Inoue, *Phys. Rev. B* **77**, 165117 (2008).
- [5] A. Fert and P. M. Levy, *Phys. Rev. Lett.* **106**, 157208 (2011).
- [6] M. Morota, Y. Niimi, K. Ohnishi, D. H. Wei, T. Tanaka, H. Kontani, T. Kimura, and Y. Otani, *Phys. Rev. B* **83**, 174405 (2011).
- [7] Y. Niimi, Y. Kawanishi, D. H. Wei, C. Deranlot, H. X. Yang, M. Chshiev, T. Valet, A. Fert, and Y. Otani, *Phys. Rev. Lett.* **109**, 156602 (2012).
- [8] P. Laczowski, Y. Fu, H. Yang, J. C. Rojas-Sánchez, P. Noel, V. T. Pham, G. Zahnd, C. Deranlot, S. Collin, C. Bouard *et al.*, *Phys. Rev. B* **96**, 140405(R) (2017).
- [9] C. Du, H. Wang, F. Yang, and P. C. Hammel, *Phys. Rev. B* **90**, 140407(R) (2014).
- [10] B. F. Miao, S. Y. Huang, D. Qu, and C. L. Chien, *Phys. Rev. Lett.* **111**, 066602 (2013).
- [11] H. Wang, C. Du, P. C. Hammel, and F. Yang, *Appl. Phys. Lett.* **104**, 202405 (2014).
- [12] D. Tian, Y. Li, D. Qu, S. Y. Huang, X. Jin, and C. L. Chien, *Phys. Rev. B* **94**, 020403(R) (2016).
- [13] S. C. Baek, V. P. Amin, Y. W. Oh, G. Go, S. J. Lee, G. H. Lee, K. J. Kim, M. D. Stiles, B.-G. Park, and K. J. Lee, *Nat. Mater.* **17**, 509 (2018).
- [14] Y. Omori, E. Sagasta, Y. Niimi, M. Gradhand, L. E. Hueso, F. Casanova, and Y. C. Otani, *Phys. Rev. B* **99**, 014403 (2019).
- [15] A. Tsukahara, Y. Ando, Y. Kitamura, H. Emoto, E. Shikoh, M. P. Delmo, T. Shinjo, and M. Shiraishi, *Phys. Rev. B* **89**, 235317 (2014).
- [16] O. Gladii, L. Frangou, A. Hallal, R. L. Seeger, P. Noël, G. Forestier, S. Auffret, M. Rubio-Roy, P. Warin, L. Vila *et al.*, *Phys. Rev. B* **100**, 174409 (2019).
- [17] W. Wang, T. Wang, V. P. Amin, Y. Wang, A. Radhakrishnan, A. Davidson, S. R. Allen, T. J. Silva, H. Ohldag, D. Balzar *et al.*, *Nat. Nanotechnol.* **14**, 819 (2019).
- [18] I. A. Campbell, A. Fert, and O. Jaoul, *J. Phys. C* **3**, S95 (1970).
- [19] N. Nagaosa, J. Sinova, S. Onoda, A. H. MacDonald, and N. P. Ong, *Rev. Mod. Phys.* **82**, 1539 (2010).
- [20] V. P. Amin, J. Li, M. D. Stiles, and P. M. Haney, *Phys. Rev. B* **99**, 220405(R) (2019).
- [21] G. Qu, K. Nakamura, and M. Hayashi, *Phys. Rev. B* **102**, 144440 (2020).
- [22] K. S. Das, J. Liu, B. J. van Wees, and I. J. Vera-Marun, *Nano Lett.* **18**, 5633 (2018).
- [23] A. Davidson, V. P. Amin, W. S. Aljuaid, P. M. Haney, and X. Fan, *Phys. Lett. A* **384**, 126228 (2020).
- [24] T. Greber, T. J. Kreutz, and J. Osterwalder, *Phys. Rev. Lett.* **79**, 4465 (1997).

- [25] M. W. Keller, K. S. Gerace, M. Arora, E. K. Delczeg-Czirjak, J. M. Shaw, and T. J. Silva, *Phys. Rev. B* **99**, 214411 (2019).
- [26] S. Eich, M. Plötzing, M. Rollinger, S. Emmerich, R. Adam, C. Chen, H. C. Kapteyn, M. M. Murnane, L. Plucinski, D. Steil *et al.*, *Sci. Adv.* **3**, e1602094 (2017).
- [27] T. J. Kreutz, T. Greber, P. Aebi, and J. Osterwalder, *Phys. Rev. B* **58**, 1300 (1998).
- [28] D. H. Wei, Y. Niimi, B. Gu, T. Ziman, S. Maekawa, and Y. Otani, *Nat. Commun.* **3**, 1058 (2012).
- [29] Y. Ou, D. C. Ralph, and R. A. Buhrman, *Phys. Rev. Lett.* **120**, 097203 (2018).
- [30] B. Gu, T. Ziman, and S. Maekawa, *Phys. Rev. B* **86**, 241303 (R) (2012).
- [31] M. Wahler, N. Homonnay, T. Richter, A. Müller, C. Eisenschmidt, B. Fuhrmann, and G. Schmidt, *Sci. Rep.* **6**, 28727 (2016).
- [32] Y. Ou, Z. Wang, C. S. Chang, H. P. Nair, H. Paik, N. Reynolds, D. C. Ralph, D. A. Muller, D. G. Schlom, and R. A. Buhrman, *Nano Lett.* **19**, 3663 (2019).
- [33] V. Marian, *Ann. Phys.* **11**, 459 (1937).
- [34] S. A. Ahern, M. J. C. Martin, and W. Sucksmith, *Proc. R. Soc. A* **248**, 145 (1958).
- [35] S. Y. Hsu, P. Holody, R. Loloee, J. M. Rittner, W. P. Pratt, and P. A. Schroeder, *Phys. Rev. B* **54**, 9027 (1996).
- [36] A. Okada, S. He, B. Gu, S. Kanai, A. Soumyanarayanan, S. Ter Lim, M. Tran, M. Mori, S. Maekawa, and F. Matsukura, *Proc. Natl. Acad. Sci. U.S.A.* **114**, 3815 (2017).
- [37] J. C. Rojas-Sánchez, M. Cubukcu, A. Jain, C. Vergnaud, C. Portemont, C. Ducruet, A. Barski, A. Marty, L. Vila, J. P. Attané *et al.*, *Phys. Rev. B* **88**, 064403 (2013).
- [38] A. Brataas, Y. Tserkovnyak, G. E. W. Bauer, and B. I. Halperin, *Phys. Rev. B* **66**, 060404(R) (2002).
- [39] J. C. Rojas-Sánchez, N. Reyren, P. Laczkowski, W. Savero, J. P. Attané, C. Deranlot, M. Jamet, J. M. George, L. Vila, and H. Jaffrès, *Phys. Rev. Lett.* **112**, 106602 (2014).
- [40] See Supplemental Material at <http://link.aps.org/supplemental/10.1103/PhysRevLett.125.267204> for the out of plane angular dependence at RT, thickness dependence of the magnetic properties, AHE, and resistivity measurements of NiCu films and heterostructures, measurement of the FMR on a large field span, and angular dependence below the Curie temperature. The Supplemental Material includes Refs. [41–44].
- [41] A. M. Abdul-Lettif, *Physica (Amsterdam)* **388B**, 107 (2007).
- [42] M. E. Fisher and J. S. Langer, *Phys. Rev. Lett.* **20**, 665 (1968).
- [43] S. K. D. Roy and A. V. Subrahmanyam, *Phys. Rev.* **177**, 1133 (1969); H. M. Ahmad and D. Greig, *J. Phys. (Paris)*, *Colloq.* **35**, C4 (1974); J. B. Sousa, M. R. Chaves, M. F. Pinheiro, and R. S. Pinto, *J. Low Temp. Phys.* **18**, 125 (1975).
- [44] K. Lenz, T. Toliński, J. Lindner, E. Kosubek, and K. Baberschke, *Phys. Rev. B* **69**, 144422 (2004).
- [45] Y. Tserkovnyak, A. Brataas, and G. E. W. Bauer, *Phys. Rev. B* **66**, 224403 (2002).
- [46] M. Caminale, A. Ghosh, S. Auffret, U. Ebels, K. Ollefs, F. Wilhelm, A. Rogalev, and W. E. Bailey, *Phys. Rev. B* **94**, 014414 (2016).
- [47] S. Andersson and V. Korenivski, *J. Appl. Phys.* **107**, 09D711 (2010).
- [48] H. Y. T. Nguyen, R. Acharyya, W. P. Pratt, and J. Bass, *J. Appl. Phys.* **109**, 07C903 (2011).
- [49] B. Dassonneville, R. Acharyya, H. Y. T. Nguyen, R. Loloee, W. P. Pratt, and J. Bass, *Appl. Phys. Lett.* **96**, 022509 (2010).
- [50] A. F. Kravets, A. I. Tovstolytkin, Y. I. Dzhezherya, D. M. Polishchuk, I. M. Kozak, and V. Korenivski, *J. Phys. Condens. Matter* **27**, 446003 (2015).
- [51] O. Gladii, L. Frangou, G. Forestier, R. L. Seeger, S. Auffret, I. Jourard, M. Rubio-Roy, S. Gambarelli, and V. Baltz, *Phys. Rev. B* **98**, 094422 (2018).
- [52] B. Heinrich, S. T. Purcell, J. R. Dutcher, K. B. Urquhart, J. F. Cochran, and A. S. Arrott, *Phys. Rev. B* **38**, 12879 (1988).
- [53] J. Lindner and K. Baberschke, *J. Phys. Condens. Matter* **15**, R193 (2003).
- [54] B. Heinrich, Y. Tserkovnyak, G. Woltersdorf, A. Brataas, R. Urban, and G. E. W. Bauer, *Phys. Rev. Lett.* **90**, 187601 (2003).
- [55] A. F. Kravets, A. N. Timoshevskii, B. Z. Yanchitsky, O. Yu. Salyuk, S. O. Yablonovskii, S. Andersson, and V. Korenivski, *J. Magn. Magn. Mater.* **324**, 2131 (2012).
- [56] E. Sagasta, Y. Omori, M. Isasa, M. Gradhand, L. E. Hueso, Y. Niimi, Y. C. Otani, and F. Casanova, *Phys. Rev. B* **94**, 060412(R) (2016).
- [57] K. P. Kämper, W. Schmitt, and G. Güntherodt, *Phys. Rev. B* **42**, 10696 (1990).
- [58] H. Hopster, R. Raue, G. Güntherodt, E. Kisker, R. Clauberg, and M. Campagna, *Phys. Rev. Lett.* **51**, 829 (1983).
- [59] M. Pickel, A. B. Schmidt, M. Weinelt, and M. Donath, *Phys. Rev. Lett.* **104**, 237204 (2010).
- [60] D. E. Shai, C. Adamo, D. W. Shen, C. M. Brooks, J. W. Harter, E. J. Monkman, B. Burganov, D. G. Schlom, and K. M. Shen, *Phys. Rev. Lett.* **110**, 087004 (2013).
- [61] T. J. Hicks, B. Rainford, J. S. Kouvel, G. G. Low, and J. B. Comly, *Phys. Rev. Lett.* **22**, 531 (1969).
- [62] Y. Ito and J. Akimitsu, *J. Phys. Soc. Jpn.* **35**, 1000 (1973).